UNIVERSITY OF LEEDS

Polyamide 6 and Thermoplastic Polyurethane Recycled Hybrid Fibres Via Twin-Screw Melt Extrusion

Siti Zaharah Kunchimon [1,2], Muhammad Tausif [1], Parikshit Goswami [3] and Vien Cheung [1]

[1] School of Design, University of Leeds, LS2 9JT, UK

[2] Department of Mechanical Engineering, Faculty of Engineering Technology, Universiti Tun Hussein Onn Malaysia, 86400, Batu Pahat, Johor, Malaysia

[3] School of Applied Science, University of Huddersfield, HD1 3DH, UK

Correspondence: Siti Zaharah (email: zahara@uthm.edu.my; tel: +447423486603)

Abstract

The sorting of multi-component textile waste into individual components limit the recycling potential of textile waste. Thermo-mechanical processes can be applied to recycle mixed waste, without sorting, to extrude hybrid fibres. This research reports on the mixing of polyamide 6 (PA6) and thermoplastic polyurethane (TPU) polymers to produce hybrid fibres by melt extrusion process. Two different blending compositions; namely PA6-80 and PA6-50, were produced. SEM images show the development of interconnected multi-porous hybrid fibre structures with average fibre and pore diameter of 126-136 µm and 7-8 µm, respectively. Differential scanning calorimetry (DSC), TGA and ATR-FTIR results show the changes in the thermal and chemical properties of the blends, demonstrating the interactions that happen between PA6 and TPU. Mechanical testing shows properties of the novel hybrid fibres are in between that of the fibres spun from the constituent polymers. The multicomponent melt extrusion can be potentially applied to the mixed polymer waste.

Keywords: Blends, fibres, thermoplastics, recycle, extrusion

Introduction

Plastic litter is a problem of growing concern around the globe. The Goal 12 of the 2030 Agenda for Sustainable Development [1] commits to responsible consumption and production. More than two-thirds of textile raw materials come from a plastic source. The increasing demand for textiles products is likely to increases the amount of plastic waste generated [2] and this is of concern, especially for materials from non-renewable sources. Globally, 92 million tonnes of clothing waste were recorded in 2015 and expected to reach 148 million tonnes by 2030 [3]. Most of the waste were sent to landfill, incinerated for energy recovery [4] or polluted the oceans in the form of microfibres [5] while only 25% were recovered through reuse and recycling routes [6]. The reuse of textile products can be a preferred option as the effective life of textile products can be extended. However, a sizeable proportion of the textile waste (usually worn out fabric, torn, stained, mildewed) inevitably needs recycling.

Textile recycling can be divided into fabric recycling, fibre recycling, polymer/oligomer recycling and monomer recycling which can be achieved by mechanical, chemical and/or thermal processes [6, 7]. Fabric recycling and fibre recycling are widely adopted in the industry. Polymer and

monomer recycling, at the moment, are limited to one material groups such as PA6 [8–10], polyester [11] and cellulose-based fibres [12, 13]. Despite the growing awareness and efforts to recycle textile waste, the amount of the waste that recycled back to produce materials for new clothing is still very small (<1%) [6]. In textile industry, blending of two or more materials (e.g. blend of polyester/cotton yarn, bi-component fibre, coated fabric) is usually performed to achieve desired end use properties. However, lack of technologies and facilities to sort and separate mixed-waste materials at an industrial scale limits the recycling of composite materials [14].

One of the approaches to recycle mixed-waste can be direct thermo-mechanical processing of the mixed-waste. The blending of two or more recycled polymers can allow the development of blended fibres in novel morphologies and with improved properties. There are two possible morphologies developed in polymer blend; matrix-dispersed structure and co-continuous structure [15]. The matrix-dispersed structure can produce varieties of dispersed shapes such as a sphere, droplet or fibril. In fibre production, the elongation force during processing forms the matrix-fibril structure. The matrix-fibril structure resembles the island-in-the-sea bi-component fibres with the fibrils resembles the 'island', and the matrix resembles the 'sea'. By removing the 'sea' or matrix during subsequent production, micro or nanofibres can be obtained [16, 17]. Meanwhile, the co-continuous structures are formed when individual polymers are connected to each other and produced a continuous structure [18, 19]. Different proportion of components and the polymer types can allow to produce varying blended fibre structures.

The applications of polyamide woven fabrics coated with thermoplastic polyurethane (TPU) include marine products such as inflatable raft, life vest and buoyancy control products [20]. Polyamide, or commonly known as nylon, ranks third among synthetic textile fibres, with 4.55 million tonnes produced in 2014 [21]. In polyamide family, polyamide 6 (PA6) dominates (86%) usage in the apparel industry compared to PA6,6 (14%) [21]. PA6 exhibits excellent mechanical, thermal and chemical resistance properties and considered as an expensive thermoplastic polymer (compared to commodity polyolefin and polyethylene terephthalate). Hence, by recycling, the life and usage of the polymer can be extended. TPU is an elastomer with high elongation, high strength, high elasticity and excellent resistance to oil, grease, solvents and chemicals [22]. Like PA6, TPU is also a highly expensive polymer. In the textiles industry, TPU is mainly used as a coating onto fabrics, and nonwoven fabrics are produced for medical, pharmaceutical, sportswear and filtration applications.

Several studies have produced hybrid fibres by blending PA6 with other materials such as low density polyethylene (LDPE) [23], cellulose acetate butyrate (CAB) [24], polypropylene (PP) [25], chitosan [26] and polyethylene terephthalate (PET) [27]. The blending of polyamide with TPU in injection moulding and compressed mould have been reported [28–32] but there is a paucity of reported work on fibre blending of PA6 and TPU. A study conducted by John and Furukawa [33] showed that PA6 fibres coated with TPU increase the tensile strength and the breaking elongation of the filaments. The blending of PA6 and TPU via melt spinning can be of further interest as the functional groups present in both polymers; hydroxyl and carbonyl groups will form hydrogen bonding with amide and urethane/urea group [34, 35].

In this study, the PA6:TPU hybrid fibres were produced by using one-step twin-screw melt spinning method. This work aims to recycle polymer waste containing more than one polymer. The approach can allow end-of-life recycling options for multi-material polymer products. The morphology,

thermal, mechanical and chemical properties of the extruded fibres were characterised. The effect of blend composition, screw speed and take-up winder speed were also studied on the fibres spun from a mix of PA6 and TPU polymers.

Materials

Extrusion grade polyamide 6 (PA6) pellets (Radilon S 35F 100NT, melting temperature: 223°C) were purchased from Radici Group, Gandino, Italy and the thermoplastic polyurethane (TPU) pellets (polyether-polyurethane type; Elastollan®1278 D 11U000, Melt flow rate: 35 g/10 min, melting temperature: 189°C) were supplied by BASF Polyurethanes GmbH, Lemförde, Germany.

Experimental

Extrusion

Hybrid fibres were extruded using a 10 mm twin-screw extruder manufactured by Rondol Technology Ltd., UK (Rondol-Microlab; screw dimension (L/D) 20:1; die diameter 2 mm). Prior to extrusion, both materials were dried in a vacuum oven (Gallenkamp, 1000 mbar) at 80°C for 6 h before mixing the two polymers (PA6:TPU) at a weight ratio of 80:20 (PA6-80) and 50:50 (PA6-50). PA6, TPU, and hybrid PA6-80 and PA6-50 were produced at 60 rpm screw speed with 24.5 m min^{-1} take-up winder speed. The temperature profile of the twin-screw extruder was divided into five heating zones and temperature profiles from the feed hopper to die were 180/200/220/225/230°C. To study the effect of screw speed and take-up winder speed, PA6-80 hybrid fibres were produced at three different screw speeds (40, 60 and 80 rpm) and take-up winder speeds of 7.5, 24.5 and 40.0 m min^{-1}. The distance between the die and take-up winder was set at 1 m. After melt spinning, the samples were conditioned at 20±2°C and a relative humidity of 65±5% for 24 h.

Characterisation of fibres

Differential Scanning Calorimetry (DSC) (heat-cool-heat, Nitrogen (N$_2$): 25 mL min^{-1}, temperature: 0-250°C, heating rate: 10°C min^{-1}) studies were performed to analyse the thermal transitions of the single component and the hybrid fibres (5-7 mg, cut from fibres, undried). Testing was conducted on a Q2000 apparatus from TA instrument. The melting and crystallisation behaviour of the fibres were observed from DSC thermograph. The percentage of PA6 crystallinity for the fibres were calculated from eq. (1) [25], where ΔH_m is melting enthalpy, w_{PA6} is the weight percentage of PA6 in the hybrid fibres and ΔH_m^0 is a reference value of melting enthalpy for PA6 (230.1 J g^{-1}) [25, 36].

$$\% \, Crystallinity \, of \, PA6 = \frac{\Delta H_m}{\Delta H_m^0 \times w_{PA6}} \times 100 \qquad (1)$$

Thermogravimetric analyser (TGA) (TA Instruments Q50) was employed to test the thermal stability of the hybrid fibres (Nitrogen (N$_2$) : 25 mL min^{-1}, temperature: 50-600°C, heating rate: 10°C min^{-1}). X-ray diffraction (XRD) (Bruker D8) was used to study the crystal form of the hybrid fibres. The measurements were taken with Cu Kα$_1$ radiation (wavelength, λ= 0.15406 nm) in the range from 5-60° at a step size of 0.05° s^{-1}. Capillary Rheometer (Bohlin, RH2000) with a 16 mm barrel and 1 mm

diameter die was used to study the apparent viscosity of the PA6 and TPU pellets at a temperature of 230°C. The barrel has three heating zones that were held constant at a designated temperature. The polymer was then extruded through the die with piston speed ranged between 5-35 mm min^{-1} resulting in an apparent shear rate of 150 to 1050 s^{-1} with an interval of 150 s^{-1}.

The morphology of the as-spun fibres was examined using a Hitachi S-2600N SEM. The fibres were placed on a 12mm diameter pinned stubs before gold coating in an Emitech K550X sputter coater. The fibres were cross-sectioned following AATCC Test Method 202159 and viewed under a light microscope (Leica M205C). Thirty pictures of each sample were analysed using ImageJ software to get the area of the fibres cross-section. Fourier Transform Infrared Spectroscopy (FTIR) equipped with Attenuated Total Reflectance (ATR) (Perkin Elmer Spectrum BX spectrophotometer) was used (4,000-600 cm^{-1} with 32 scans, 4 cm^{-1} and scanning interval was 2 cm^{-1}) to study the infrared spectrum of the as-spun fibres. Tensile strength (cN tex^{-1}) and elongation at break (%) of single fibres were measured (gauge length: 100 mm at 500 mm min^{-1} cross-head speed) using single column tensile strength tester (Instron 5540) following BS EN 13895. 10 specimens were tested for each fibre to get an average value.

Results and Discussion

The properties of the hybrid fibres are discussed in this section including the thermal, rheology, morphology of the fibres, chemical and mechanical properties.
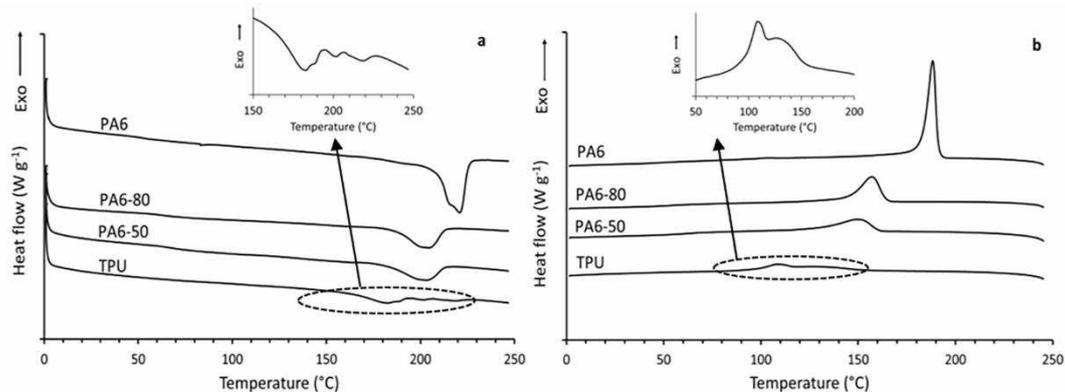
Thermal properties

Fig. 1 The DSC thermograph of; a) second heating and b) cooling scan of pure and hybrid fibres.

Table 1 Thermal properties of pure and hybrid fibres.

Fibre	Melting temperature, T_m (°C)	Melting enthalpy, ΔH_m (J g^{-1})	Crystallisation temperature, T_c (°C)	PA6 crystallinity (%)
PA6	221	59.6	188	25.9
PA6-80	204	25.9	153	14.1
PA6-50	204	24.1	148	20.9

TPU	182	9.0	108	-

The DSC curves for PA6, TPU, PA6-80 and PA6-50 fibres are shown in Fig. 1 and the melting and crystallisation behaviours are presented in Table 1. The first heating scan was conducted to remove previous thermal history. Therefore the melting temperature and melting enthalpy of the fibres were determined from the second heating scan as shown in Fig. 1a.

The PA6 melting curve shows the maximum melting peak (T_m) at 221°C, and a shoulder peak appears near to the maximum melting peak. The appearance of the shoulder could be attributed to either the development of two different crystal morphologies in the PA6 polymer or could be attributed to recrystallisation effect after the first heating cycle [37] or same kind of crystal formation with different thicknesses [38]. Two kinds of crystal forms can be expected in PA6 structure, α and γ-form, which were melted at 222°C and 213°C, respectively [39]. TPU fibres showed a melting peak at 182°C and small endothermic peaks at 202°C and 220°C. TPU is an amorphous polymer and these peaks are related to the disordering of crystallinity of TPU hard segments [40].

PA6-80 and PA6-50 show similar melting behaviour with melting temperatures at 204°C and melting enthalpy of 25.9 and 24.1 J g^{-1}, respectively. The melting point of hybrid fibres were lower than that of PA6 with a small endothermic peak of TPU. The decrease in the melting temperature of hybrid fibres can be linked to the interactions between amide group and urethane/urea group via hydrogen bonding [35]. PA6 and TPU could form extensive hydrogen bonding due to their chemical structures and availability of relevant functional groups [34, 41]. The appearance of single endotherm in the hybrid fibres indicate the existence of extensive interactions between PA6 and TPU. These two polymers, due to extensive hydrogen bonding, develops strong interactions during melt spinning thus will affect the morphological structure of the blended fibres.

The addition of 20% TPU in PA6 does affect the molecular and crystalline structure of the hybrid fibres significantly as could be seen from Table 1. The fibre blend with 1:1 composition of PA6 and TPU also affect the crystallinity of the hybrid fibres but, interestingly, shows better crystallinity than PA6-80. These results correspond with the tensile properties of the hybrid fibres; this will be discussed in Mechanical properties.

The crystallisation temperatures of the hybrid fibres are in between that of PA6 and TPU fibres (Fig. 1b) The crystallisation temperatures of PA6-80, PA6-50 and PA6 are 153°C, 148°C, and 188°C (Table 1), respectively. TPU cooling curve shows two crystallisation peaks at 108°C and 128°C which corresponding to the soft segment of TPU [31]. The blending of PA6 and TPU might disorder the PA6 crystal form [32], discussed further in Chemical properties.
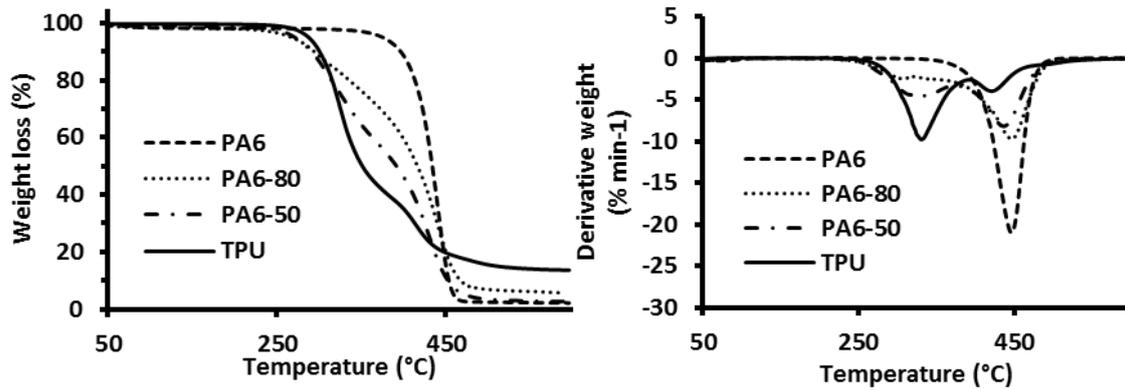
Fig. 2 TG and DTG curves of pure and hybrid fibres.

The results for thermal stability of the hybrid fibres and single component fibres are shown in Fig. 2 and Table 2. The thermal stability of hybrid fibres were in between that of pure PA6 and TPU, depending on the actual ratio of the blend components; PA6-50 started to decompose much earlier than that of PA6-80. . As TPU was found dispersed in the PA6 matrix, this helped to delay the degradation of the TPU in the blend, as evident by the T_{onset}. The degradation of 100% TPU samples happens in two steps which can be attributed to the presence of incompatible hard and soft segments of TPU.

Table 2 Thermal characteristics of pure and hybrid fibres

Fibre	T_{onset} (°C)	T_{50} (°C)	T_{max} (°C)
PA6	419	441	465
PA6-80	373	416	462
PA6-50	345	390	456
TPU	298	351	426

XRD

Diffraction spectra of the fibres are depicted in Fig. 3. For PA6, two type of crystals frequently observed are α-type and γ-type crystal structure. As displayed in PA6 spectra (Fig. 3), one sharp peak at 21.3° was obtained representing the PA6 γ-crystal structure. γ-form crystal is more pronounced in PA6 due to the moderate fibre spinning process used in this study with take-up speed less than 6 km min^{-1}.[42] TPU fibres showed amorphous peak at 20.6°. The addition of 20% of TPU in the hybrid fibres distorted the PA6 crystal form but γ-crystal remained as main crystal structure form with a very small proportion of α-type crystal. On the other hand, PA6-50 crystallised into $α_1$ and $α_2$ crystal structures which showed peaks at 20.5° and 22.7°, respectively. Interestingly, two new peaks appear on PA6-50 at peaks 14° and 17° which can be linked to the crystallinity of the hard segment of TPU [43]. Development of TPU hard

6

segment crystals in PA6-50 increases the strength of the fibres and is further discussed in mechanical properties section.
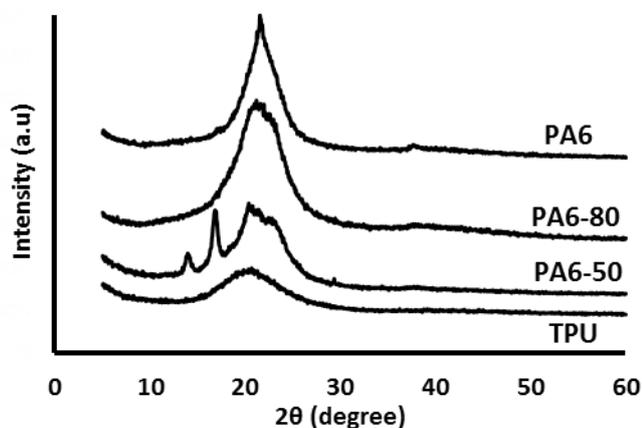

Fig. 3 XRD pattern of pure and hybrid fibres

Rheology

Flow behaviour of polymer melt depends on the shear rate, shear stress and the residence time of the polymer in the extruder [44]. The apparent viscosity of a polymer, at a given temperature, affects the distribution of the polymers in the melt extruder barrel and consequently affects the morphology and structural properties of the as-spun fibres [45–47]. In a polymer blend, the composition of each blend (blend ratio) affect the final morphology of the fibre. A polymer with a high composition will act as the matrix, and the polymer with lower composition will be the disperse component. The minor component will disperse in the primary component and will form small droplets that can be transformed into fibrils when the elongational forces were applied. The diameter of the droplets increases with the increase in the disperse phase composition [45]. The viscosity ratio of the dispersed phase to matrix phase will also affect the diameter of the droplets. Increase in dispersed component viscosity increases the viscosity ratio of dispersed to matrix phase thus increases the average diameter of the droplet but reduces the number of droplets formed. Therefore, to measure the viscosity ratio of the studied polymers, the estimated viscosity of the polymers during melt spinning are determined by considering the screw speed of the extruder during melt processing.

The screw speeds for the production of PA6:TPU hybrid fibres were set at 40, 60 and 80 rpm. The shear rate for each conditions were calculated using eq. (2) [48] where D is a screw outside diameter, n is a screw speed (rpm) and h is an overflight gap between the tip of the screw and the inner wall of the barrel.

In this study, the screw diameter is 10 mm, and the overflight gap is 0.1 mm. The calculated shear rate for the hybrid polymer of PA6 and TPU processing at 40, 60 and 80 rpm are 209, 314 and 419 s^{-1} respectively.

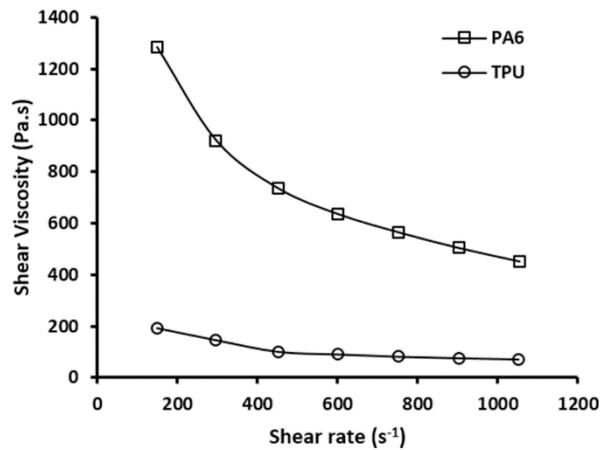$$Shear\ rate = \frac{\pi \times D \times n}{h \times 60} \tag{2}$$

Fig. 4 The shear viscosity-shear rate of PA6 and TPU at 230°C.

As can be seen from Fig. 4, both polymers are non-Newtonian fluids with shear thinning fluid characteristic, where the viscosity of both polymers decreased with increasing shear rate. PA6 showed higher viscosity compare to the TPU, which can be attributed to the dissimilar melting temperatures of both polymers. TPU melting temperature is 189°C and therefore will show lower viscosity at 230°C compared with PA6 which completely melt at 220°C. The shear rate of 209, 314 and 419 s^{-1} for PA6:TPU hybrid fibres processed at 230°C corresponds to the viscosities of PA6 (1130, 890 and 770 Pa.s) and TPU (170, 120 and 100 Pa.s). Therefore, the viscosity ratio of the hybrid polymer is 0.15, 0.13 and 0.12 for the shear rates 209 s^{-1}, 314 s^{-1} and 419 s^{-1}, respectively, evaluated using eq. (3). The lower viscosity ratio should lead to finer droplets of the dispersed phase in the polymer blend. Increasing the screw speed (rpm) results in increasing the shear rate thus contributes to the better dispersion of the blend [49]. Increasing shear rate has been reported to cause a decrease in the diameter of the fibrils [45] from dispersed droplets.

$$Viscosity\ ratio = \frac{viscosity\ dispersed, \eta_d}{viscosity\ matrix, \eta_m} \tag{3}$$

Morphology of the hybrid fibres

The formation of the sphere, laminar or fibril morphologies might happen in a polymer blend [45]. However, in this study, the phase separation between PA6 and TPU was not clearly observed in both hybrid fibres, PA6-80 and PA6-50, as shown in Fig. 5. In other studies involving the blending of TPU with PA6 [30], PA10 [29], PA11 [31] and PA1212 [28], the separation between these two polymers were observed under SEM.
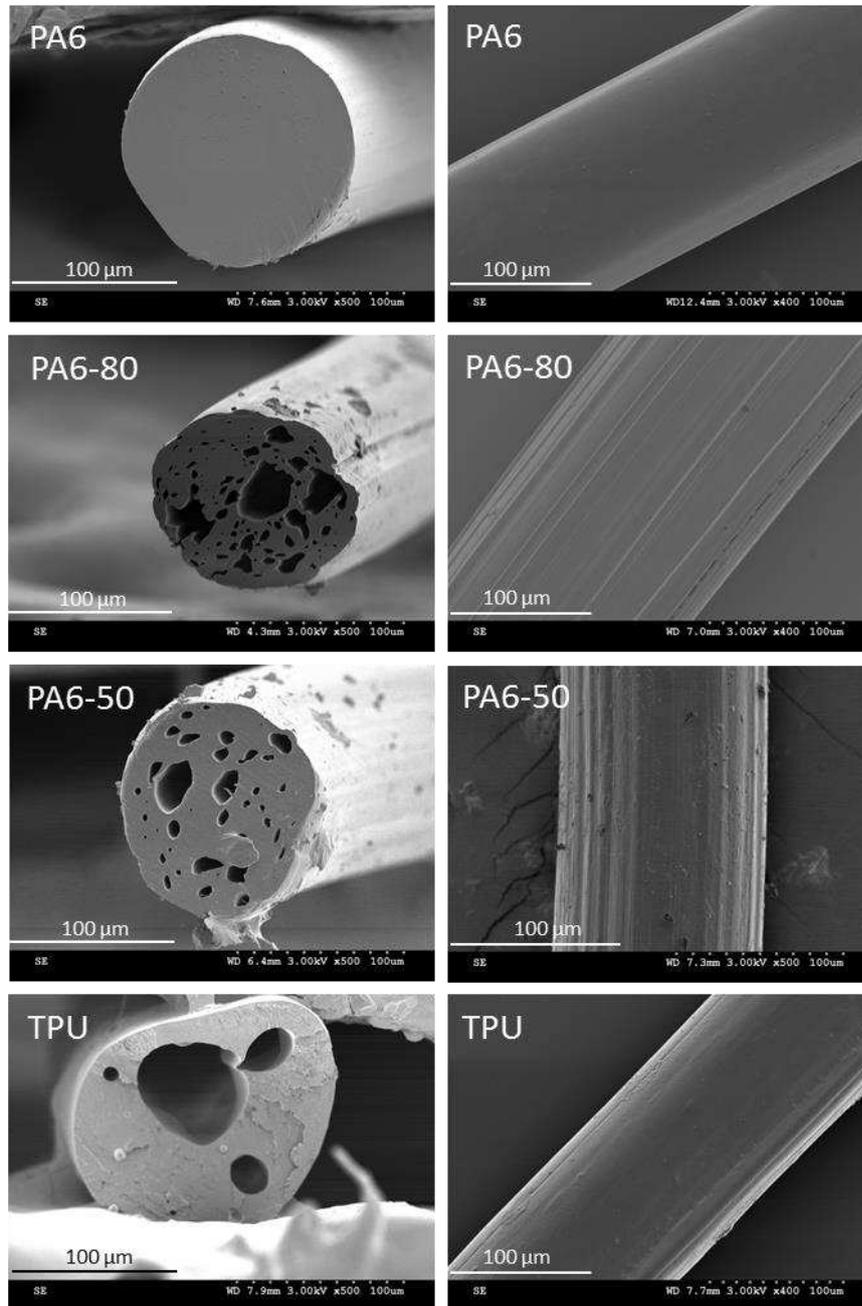
Fig. 5 SEM micrograph of fibre's cross-section (left) and fibre surface (right).

Distinct morphology differences can be observed between the single component and hybrid fibres, as shown in Fig. 5. PA6 fibre shows a clean and smooth cross-sectional and longitudinal view. Rod-like appearance can be seen from the image, as expected from PA6 fibres. When 20% of TPU was added, porous fibres with rough and grooved surface were formed. For the PA6-50 hybrid fibre, the existence of pores still can be observed with the fibre surface smoother than PA6-80.

The porous features are also evident in TPU fibres processed at 230°C. To critically understand the formation of the TPU porous structures, TPU fibres were extruded at different temperatures (200°C to 230°C). Fig. 6 shows that the pores started to appear in the TPU fibres produced at 220°C and the

significant appearance of pores can be seen in the TPU fibres produced at 230°C. The processing of TPU at high temperature (~230°C) can lead to degradation of TPU owing to oxidation, chain scission and release of carbon dioxide [50]. The pores that appear in TPU and hybrid fibres could be attributed to the formation of gas bubbles which were produced during the melt spinning process. Chiu and Chuang [30] studied the mechanical properties of the compressed mould of PA6:TPU (80:20) and found the presence of small holes that cause a decrement in tensile stress. Other study conducted by Zo et al. [35] also reported the development of small holes in the PA6 and TPU blend composites. Both studies prepared the PA6:TPU blends at the temperature range of 230 to 260°C.

The processing temperature of TPU in this study is higher than the average melting temperature of TPU (~185°C) and this causes the degradation of TPU and thus could cause the pores in the hybrid fibres. The presence of the pores in the single component TPU fibres at higher processing temperature (Fig. 6) explains the formation of the pores in the PA6:TPU hybrid fibres.
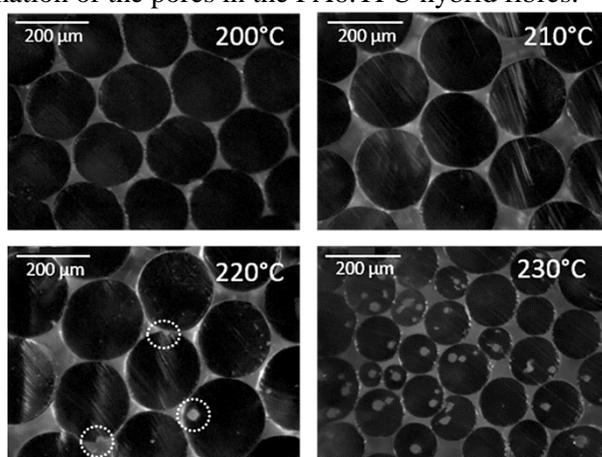

Fig. 6 Microscope images of TPU produce at 200°C to 230°C (dotted circles in 220°C image show the pores appear in the fibre).

To further investigate the morphology of the hybrid fibres, the single component fibres and hybrid fibres were treated with dimethyl sulfoxide (DMSO) for 24 h at room temperature with the aim to remove the TPU component. During the treatment, TPU fibres were dissolved after 15 mins in DMSO. The hybrid fibres and PA6 remained in the fibre form after 24 h of treatment. As shown in Fig. 7, the morphology of the DMSO-treated hybrid fibres changed when compared with untreated fibres, thus proving the presence of the TPU in the as-spun hybrid fibres. The morphology of the hybrid fibres after the treatment with DMSO can be assumed as a matrix-disperse phase; with PA6 as the matrix while TPU act as the disperse phase. Previous studies show the apparent shape of TPU dispersed in polyamide matrix, with the dispersed is in the sphere [28, 31] and sphericity [29] shape.
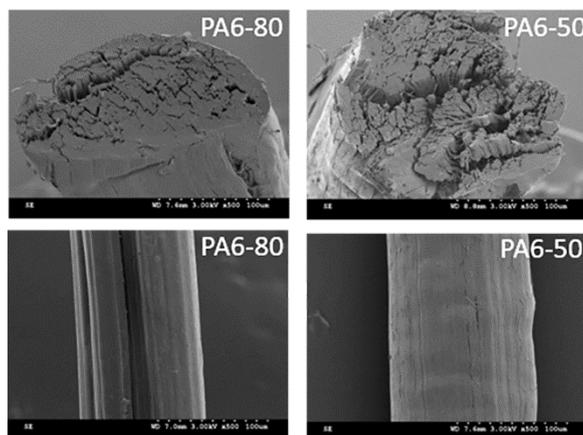
Fig. 7 SEM images of hybrid fibres after treated with DMSO for 24 h. (Upper images: cross-sectional view, bottom images: fibre longitudinal view). The images before DMSO-treatment are reported in Fig. 4.

The PA6-80 hybrid fibres were also produced at different screw speed settings (40, 60 and 80 rpm) with two take-up winder speeds (24.5 and 40 m min^{-1}) to investigate the influence of processing parameters on the morphology of the hybrid fibres. From Fig. 8 and Fig. 9, it could be seen that the pores exist in all the fibres independent of the processing parameters. Besides, uneven and groove-like fibre surface morphology can be seen on hybrid fibres, compared with the single component fibres that have relatively smooth fibre surfaces (Fig. 5). The uneven surfaces can offer higher surface area compared to relatively smooth fibres making them highly desirable for technical applications such as filtration.
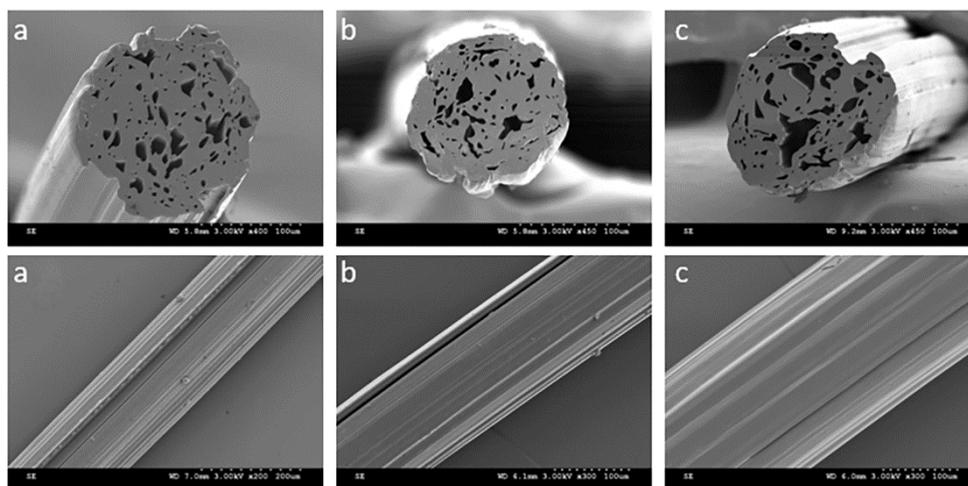

Fig. 8 SEM images of PA6-80 produced with the same winder take-up speed (24.5 m min^{-1}) and different screw speed; a) 40, b) 60 and c) 80 rpm. (Upper images: cross-sectional view, bottom images: fibre longitudinal view)
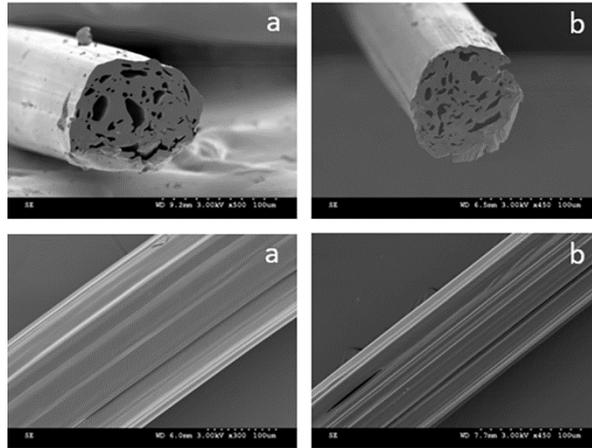
12

Fig. 9 SEM images of PA6-80 produced with the same screw speed 80 rpm and different winder take-up speed; a) 24.5 m min^{-1} and b) 40 m min^{-1}. (Upper images: cross-sectional view, bottom images: fibre longitudinal view)
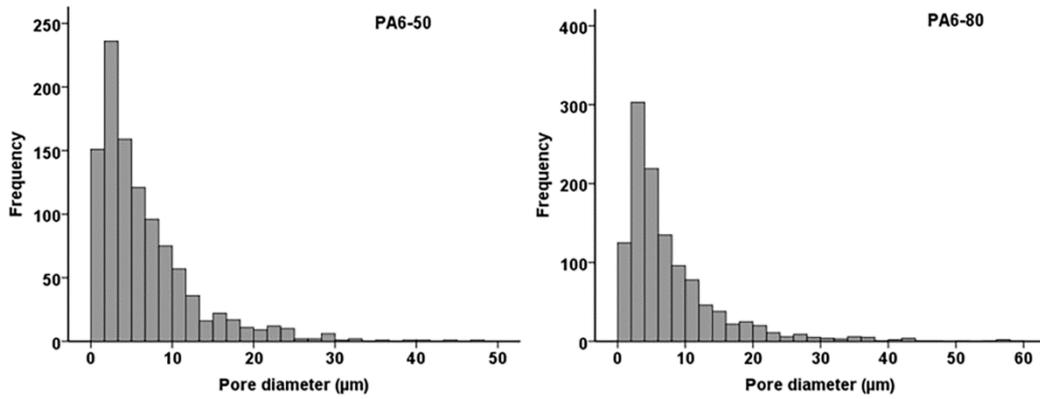

Fig. 10 The pore diameter distribution of hybrid fibres. (n_{PA6-50}=1046, n_{PA6-80}=1170, obtained from 30 specimens for each blend)
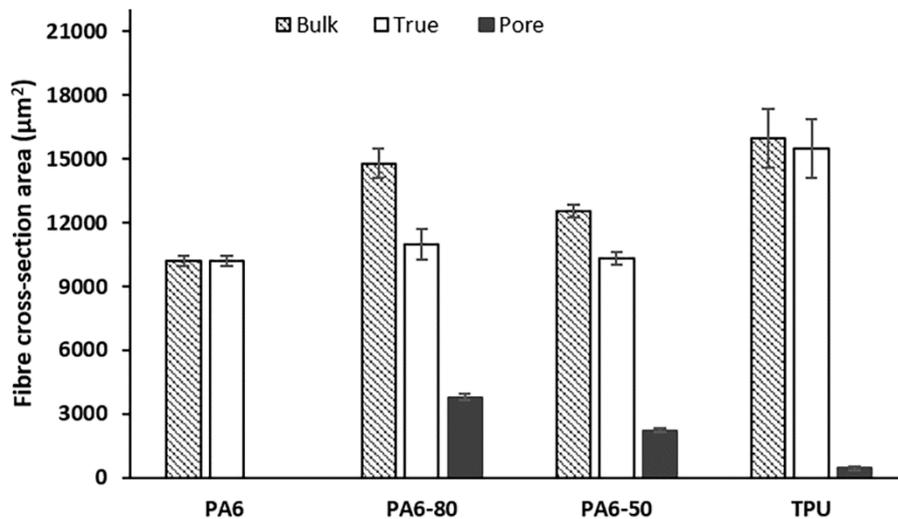

Fig. 11 The fibre cross-sectional area (bulk and true), total pore area of pure and hybrid fibres. (n=30)

Owing to non-circular cross-section shape of the as-spun hybrid fibres, the "circular equivalent diameter" (CED) of the fibres were calculated by using eq. (4) [16] with d is a fibre diameter and A is a fibre cross-sectional area (bulk). The average diameter of PA6, PA6-80, PA6-50 and TPU fibres was 114±1.2, 136±3.2, 126±1.5 and 151±6 µm, respectively. The diameter of pores developed in the PA6-80 and PA6-50 fibres were 8 and 7 µm, respectively, calculated using eq. (4). The pore diameter distribution is shown in Fig. 10.

$$d_{CED} = \sqrt{\frac{4A}{\pi}} \tag{4}$$

Fig. 11 shows the bulk and true cross-sectional areas of the fibres, and the average pore areas. TPU showed the highest fibre cross-sectional area, followed by PA6-80, PA6-50 and PA6. The true cross-sectional areas were measured using eq. (5) and is illustrated in Fig. 12.
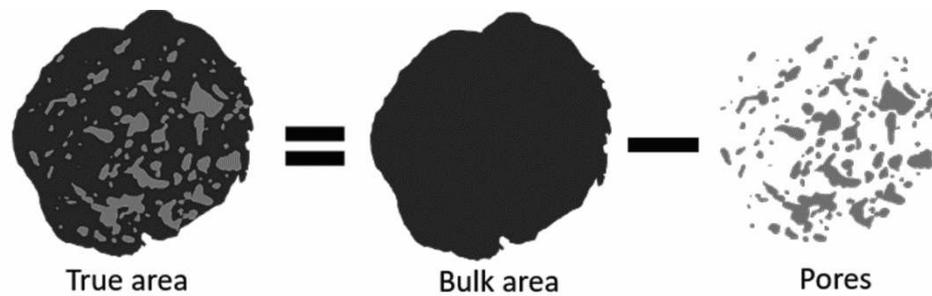

Fig. 12 Illustration of bulk and true cross-section area.

$$True\ cross-sectional\ area = Bulk\ area - total\ pores\ area \tag{5}$$

The bulk areas of the hybrid fibres are bigger than that of PA6 and smaller than TPU single component fibres. However, the true cross-sectional areas of the hybrid fibres are similar to PA6 fibres. It could be assumed that the pores developed in the hybrid fibres make the fibre cross-sectional areas expand thus having bigger bulk cross-sectional areas than single component PA6 fibres. The average of pore areas in both hybrid fibres were larger than the pore area in TPU fibre with PA6-80 showing higher pore area than PA6-50. From Fig. 13, it could be observed that significant pores were developed in PA6-80. The number and size of the pores play an important role when considering the end application of the fibres such as insulating materials, moisture absorber, filtration and more.
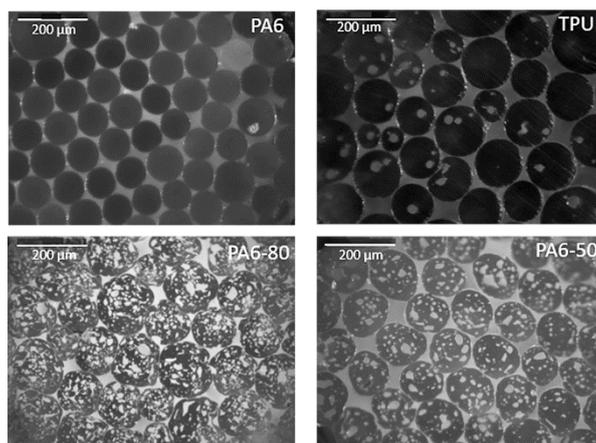
Fig. 13 Microscope images of pure and hybrid fibres.
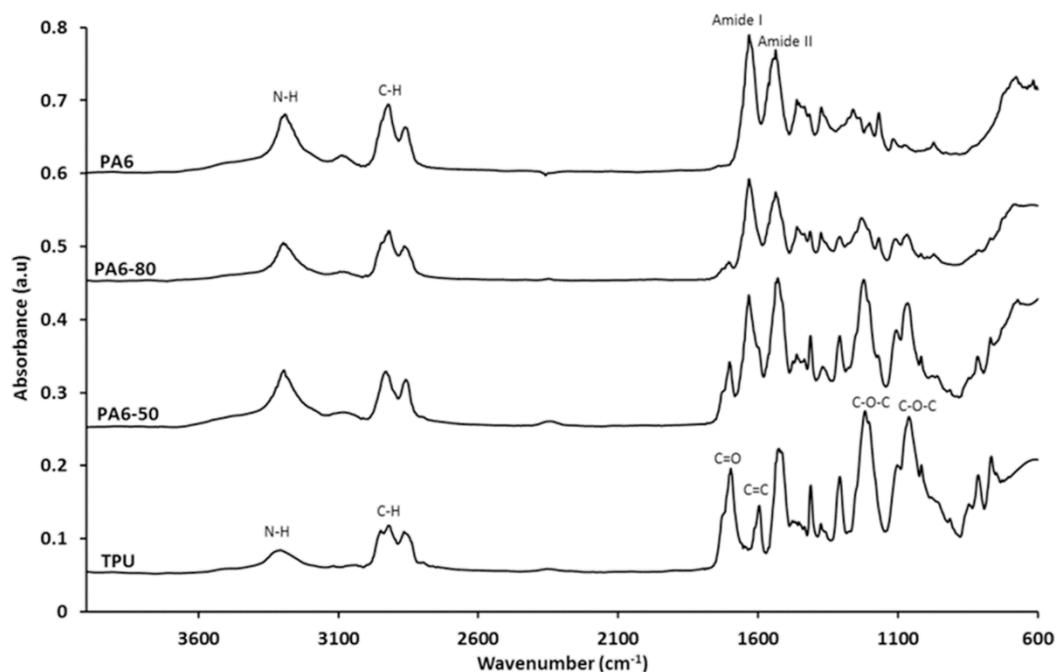
Chemical properties

Fig. 14 ATR-FTIR spectra of PA6, TPU and hybrid fibres.

The chemical structure of the hybrid fibres were compared with the single component fibres to identify any possible interactions between the two constituent polymers (Fig. 14). The PA6 components (N-H (3291 cm^{-1}), C-H (2922 & 2864 cm^{-1}), amide I (1633 cm^{-1}) and amide II (1538 cm^{-1})) as well as the TPU components (C=O (1698 cm^{-1}) and C-O-C (1218 & 1062 cm^{-1})) were observed in the hybrid fibres.

The carbonyl group (C=O, 1698 cm^{-1}) was observed in the hybrid fibres, but the peaks slightly shifted to 1705 cm^{-1} and 1703 cm^{-1} for PA6-80 and PA6-50, respectively (Fig. 15 normalised at 2866 cm^{-1}). The carbonyl region of TPU can be related to the crystalline region of urethane and urea groups

[51]. The free urea (keto group C=O) in TPU fibres changes to H-bonded urethane in both the hybrid fibres. The shifting of this peak can be associated with hydrogen bonding interactions between urea group of TPU and amide group of PA6 [31, 41]. The absorbance intensity in the carbonyl region was analysed to investigate the effect of the blend to the groups reported in Table 3. The absorbance intensity of the hybrid fibres show reduction when compared to TPU fibres, which can be related to the weight composition of the TPU in the blends. As this absorbency relates to the crystalline region of the TPU, decreasing the amount of TPU in the blend decreases the absorbency intensity.
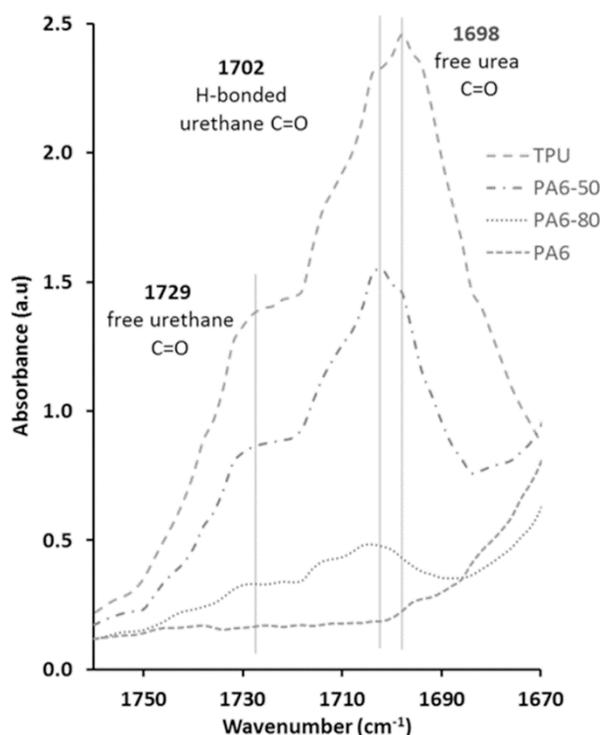

Fig. 15 The carbonyl region of TPU and hybrid fibres.

Table 3 Absorbance intensity of the fibres referring to carbonyl phase.

C=O phase	Wavenumber (cm^{-1})	Absorbance Intensity		
		TPU	PA6-50	PA6-80
Free urethane	1729	1.38	0.86	0.33
H-bonded urethane	1702	2.33	1.55	0.48
Free urea	1698	2.46	1.46	0.43

As discussed earlier in Thermal properties, the crystallinity of the hybrid fibres were lower compared to the single component fibres. α and γ- crystal form of PA6 [41] is shown in Fig. 16 (850 to 1150 cm^{-1}); the observed peaks at 1630, 1169 and 973 cm^{-1} indicate the presence of γ-form crystal whilst the α-form crystal peak could be observed at 1202 cm^{-1}. The γ-form observed at 1630 cm^{-1} can be observed in both PA6-80 and PA6-50 hybrid fibres. The α-form crystal observed at 1202 cm^{-1} in single

component PA6 fibres were not present in the hybrid fibres. The small peak at 1169 cm^{-1} appears for PA6-80 but not for PA6-50; the same is also observed with γ-form peak at 973 cm^{-1}. The blending of PA6 and TPU at high temperature might have disordered the PA6 crystal form and affected the crystallisation of the hybrid fibres.
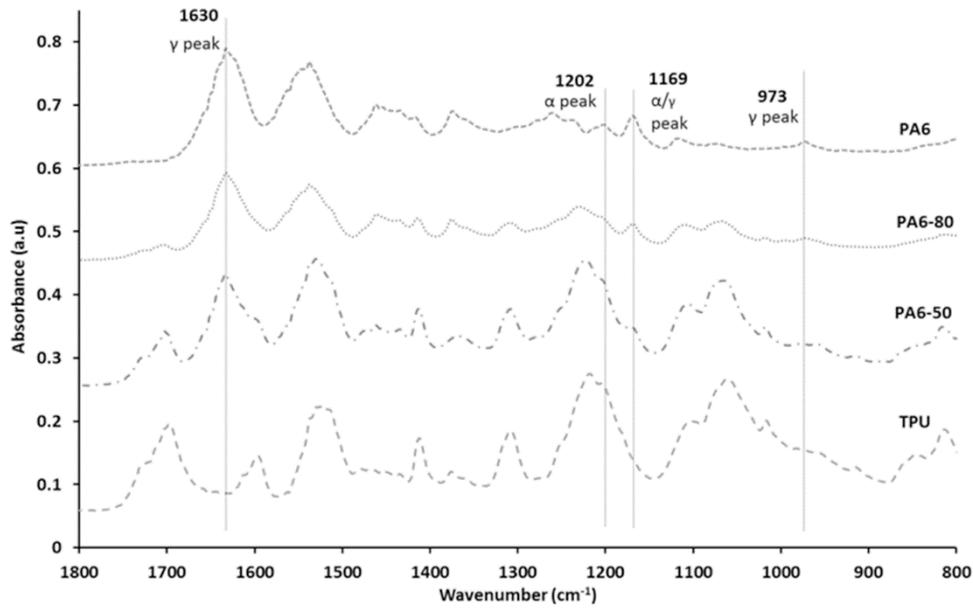

Fig. 16 FTIR spectra of α and γ-crystal form of the fibres.
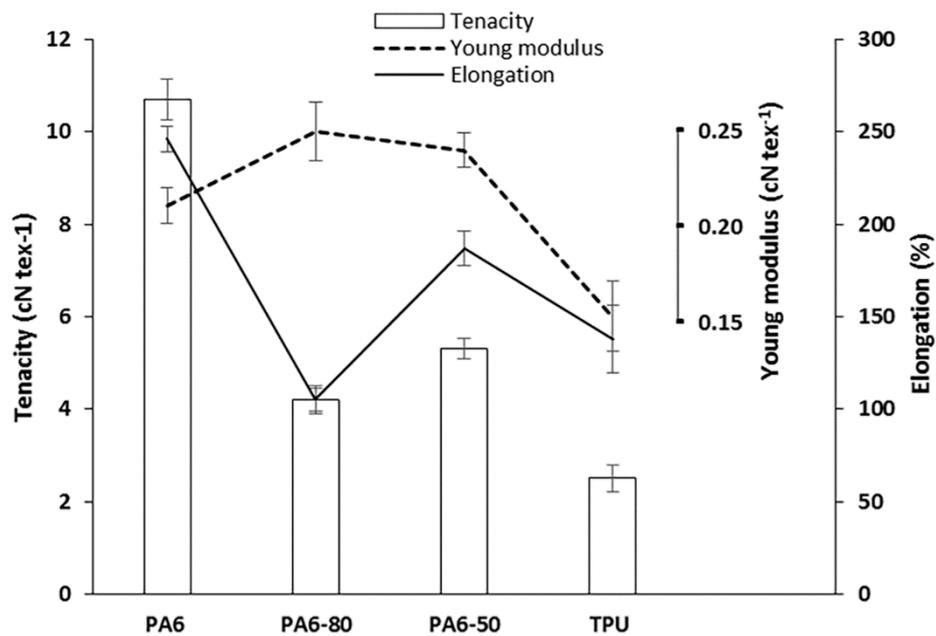
Mechanical properties

Fig. 17 Tenacity, elongation and Young modulus of PA6, TPU and hybrid fibres. (n=10)
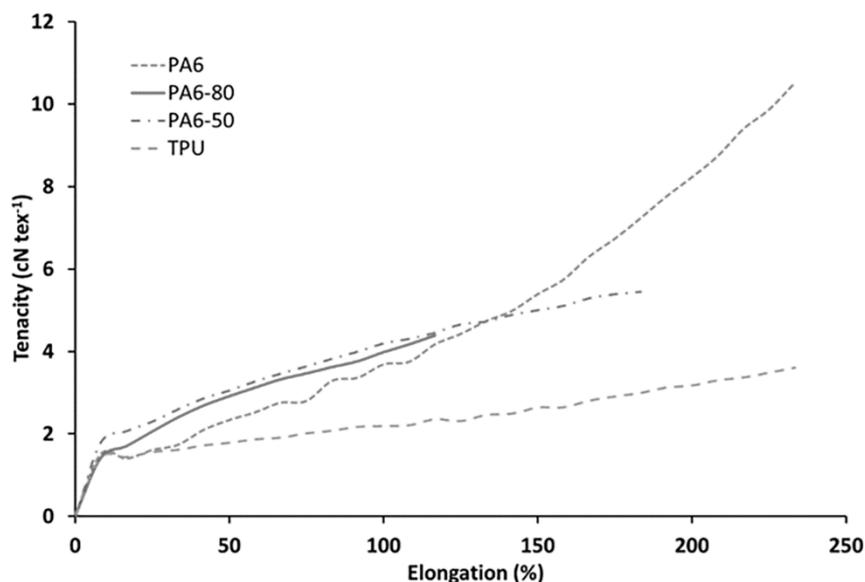
Fig. 18 The representative curve of tenacity-breaking elongation of PA6, TPU and hybrid fibres.

The blending of two different polymers is likely to alter the mechanical behaviour of the resultant hybrid fibre. Morphology and the interfacial surface tension of the polymers are the factors that affect the mechanical behaviour of the hybrid fibres [45]. The strength of the hybrid fibres can be controlled by selecting the right blend composition, either to produce a matrix-dispersed phase or co-continuous phase morphology; the latter can offer better mechanical properties but can pose processing challenges [18]. The tenacity and breaking elongation of the single component and hybrid fibres are shown in Fig. 17, and the representative tenacity-elongation curves are shown in Fig. 18.

As expected, the mechanical behaviour of the hybrid fibres lie between that of the PA6 and TPU single component fibres, with PA6-50 exhibiting superior tenacity and elongation than PA6-80. The existence of the pores introduce a weak link and this results in the reduction of the mechanical performance of the hybrid fibres. This result correspond with the mechanical properties of the PA6:TPU blend obtain by Chiu and Chuang [30]. A study by Baiju et al. showed that coating of TPU film onto PA6 fibre delayed the micro-crack formation on the PA6 fibre surface, which consequently improved the fibre strength [52]. In this research, the TPU component was dispersed inside the PA6 matrix, as demonstrated by immersion of the hybrid fibres in DMSO (**Fig. 7**). The structural position of the TPU within the PA6 matrix did not aid on delaying crack formation on the fibre surface.

Besides, the percentage of crystallinity mentioned in the thermal properties discussion can also be related to the tensile strength of the fibres. In the analysis of the thermal properties, it was found that PA6-80 hybrid fibres exhibit lower crystallinity than PA6-50. Crystallinity relates to the compactness of the lamella structure in the polymer, lesser the crystallinity, lower should be the strength of the fibres [53]. The development of TPU hard segments crystal also contributes to the strength increment in PA6-50.

The interfacial surface adhesion between PA6 and TPU can also possibly be contributing to the strength of the hybrid fibres. PA6 and TPU, as discussed earlier, could form hydrogen bonding;

however, the significant number of pores developed in the PA6-80 weaken the structures and decrease the tensile strength.

The Young's modulus of hybrid fibres are slightly higher than the single component fibres, and the breaking elongations are significantly lower than the PA6 single component fibres; PA6-80 fibres particularly show signification reduction in the elongation at break. The strong hydrogen bonding in the hybrid fibres restricts the movement of the molecules and therefore reduces the elongation at break [51]. The strength and elongation of TPU fibres processed at 230ºC are 196% and 62%, respectively, lower than the fibres processed at 200°C (Fig. 19). The high processing temperature significantly affects the strength of TPU. Therefore, it could be concluded that the reduction in the strength of the hybrid fibres is also affected by processing PA6 with TPU at high temperature.
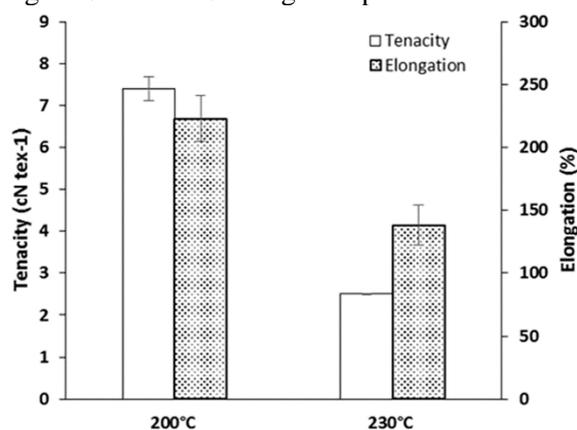

Fig. 19 Tenacity and breaking elongation of TPU fibres produce at 200°C and 230°C.

Conclusions

This work presents an approach to recycle multi-component blended textile waste for value-added applications. Although this research uses PA6 and thermoplastic polyurethane blends, this approach can be extended to other waste mixtures to produce hybrid functional fibres. Interconnected multi-pores fibres with a non-circular cross-section were produced in this study by blending PA6 and TPU at a processing temperature of 230°C; both PA6-80 and PA6-50 hybrid fibres show the existence of multi-pores. The multi-porous structure in the hybrid fibres were also observed when different take-up speeds and screw speeds were used during fibre production. The thermal analysis shows PA6 and TPU might develop strong interactions thus affecting the molecular and crystalline structure of the hybrid fibres. This was also substantiated with the chemical analysis. The mechanical analysis shows a decrease in the hybrid fibre strength compared to PA6 fibres but the hybrid fibres show better strength than TPU fibres, processed at the same temperature. The decreasing mechanical behaviour of the hybrid fibres compared to the PA6 was expected due to the formation of pores in the hybrid fibres. This study shows the feasibility of producing multi-porous high functional fibres using a conventional melt spinning method.

References

1. United Nations (2018) The Sustainable Development Goals Report
2. Bartl A (2011) Textile waste. In: Letcher TM, Vallero DA (eds) Waste: A Handbook of Management. Elsevier B.V., pp 167–179
3. Global Fashion Agenda, The Boston Consulting Group I (2017) Pulse of the Fashion Industry
4. Zainab ZI, Ali RT (2016) Recycled medical cotton industry waste as a source of biogas recovery. J Clean Prod 112:4413–4418. https://doi.org/10.1016/j.jclepro.2015.06.069
5. Falco F De, Gullo MP, Gentile G, et al (2018) Evaluation of microplastic release caused by textile washing processes of synthetic fabrics. Environ Pollut 236:916–925. https://doi.org/10.1016/j.envpol.2017.10.057
6. Ellen MacArthur Foundation (2017) A New Textiles Economy: Redesigning Fashion's Future. https://www.ellenmacarthurfoundation.org/publications. Accessed 20 Aug 2018
7. Sandin G, Peters GM (2018) Environmental impact of textile reuse and recycling – A review. J Clean Prod 184:353–365. https://doi.org/10.1016/j.jclepro.2018.02.266
8. Econyl Some see trash. Others see treasure. http://www.econyl.com/the-process/. Accessed 31 Aug 2018
9. Repreve Grow your brand with REPREVE. https://repreve.com/business-solutions. Accessed 31 Aug 2018
10. Toray (2011) Toray Draws Up Strategy to Expand Fibers and Textiles Recycling Business. https://www.toray.com/news/eco/nr111021.html#/. Accessed 31 Aug 2018
11. Teijin The Outstanding Potential of Teijin's ECO CIRCLE™ System
12. Evrnu (2016) Evrnu™ and Levi Strauss & Co. Create First Jeans Made From Post-Consumer Cotton Garment Waste. http://www.evrnu.com/blog/. Accessed 4 Jul 2016
13. Re:newcell We Make Fashion Sustainable. https://renewcell.com/. Accessed 31 Aug 2018
14. Östlund Å, Wedin H, Bolin L, et al (2015) Textilåtervinning Tekniska möjligheter och utmaningar [Tetxile recycling-technical opportunities and challanges]. In: Naturvårdsverket. https://www.naturvardsverket.se/Documents/publikationer6400/978-91-620-6685-7.pdf?pid=15536. Accessed 20 Aug 2018
15. Wang L, Guo Z-X, Yu J (2012) Cocontinuous Phase Morphology for an Asymmetric Composition of Polypropylene/Polyamide 6 Blend by Melt Mixing of Polypropylene with Premelted Polyamide 6/Organoclay Masterbatch. J Appl Polym Sci 123:1218–1226. https://doi.org/10.1002/app.34600
16. Tran NHA, Brünig H, Auf der Landwehr M, et al (2016) Controlling micro- and nanofibrillar morphology of polymer blends in low-speed melt spinning process. Part II: Influences of extrusion rate on morphological changes of a PLA/PVA blend through a capillary die. J Appl Polym Sci 133:1–10. https://doi.org/10.1002/app.44257
17. Tran NHA, Brünig H, Heinrich G (2016) Controlling micro- and nanofibrillar morphology of polymer blends in low-speed melt spinning process . Part I . Profiles of PLA / PVA-filament parameters along the spinline. J Appl Polym Sci 1–14. https://doi.org/10.1002/app.44258
18. Pötschke P, Paul DR (2003) Formation of Co-continuous Structures in Melt-Mixed Immiscible Polymer Blends. J Macromol Sci Part C Polym Rev 43:87–141. https://doi.org/10.1081/MC-120018022
19. Willemse RC, Posthuma De Boer A, Van Dam J, Gotsis AD (1999) Co-continuous morphologies in polymer blends: The influence of the interfacial tension. Polymer (Guildf) 40:827–834. https://doi.org/10.1016/S0032-3861(98)00307-3
20. Erez (2018) 2018 Technology Report for Marine Safety Textiles
21. Wesołowski J, Płachta K (2016) The polyamide market. Fibres Text East Eur 24:12–18.

https://doi.org/10.5604/12303666.1215537

22. Huntsman (2010) A guide to thermoplastic polyurethanes (TPU)

23. Pan Z, Chen Y, Zhu M, et al (2010) The non-uniform phase structure in blend fiber. II. The migration phenomenon in melt spinning. Fibers Polym 11:625–631. https://doi.org/10.1007/s12221-010-0626-3

24. Zhang P, Xu D, Xiao R (2015) Morphology development and size control of PA6 nanofibers from PA6/CAB polymer blends. J Appl Polym Sci 132:1–8. https://doi.org/10.1002/app.42184

25. Afshari M, Kotek R, Gupta BS, et al (2005) Mechanical and structural properties of melt spun polypropylene/nylon 6 alloy filaments. J Appl Polym Sci 97:532–544. https://doi.org/10.1002/app.21772

26. Dotto G., Santos JMN, Tanabe EH, et al (2017) Chitosan/polyamide nanofibers prepared by Forcespinning®technology: A new adsorbent to remove anionic dyes from aqueous solutions. J Clean Prod 144:120–129. https://doi.org/10.1016/j.jclepro.2017.01.004

27. Aslan S, Laurienzo P, Malinconico M, et al (1995) Influence of spinning velocity on mechanical and structural behavior of PET/nylon 6 fibers. J Appl Polym Sci 55:57–67. https://doi.org/10.1002/app.1995.070550106

28. Li W, Liu J, Hao C, et al (2008) Interaction of thermoplastic polyurethane with polyamide 1212 and its influence on the thermal and mechanical properties of TPU/PA1212 blends. J Polym Eng Sci 249–256. https://doi.org/10.1002/pen.20853

29. Zhang SL, Wang G Bin, Jiang ZH, et al (2005) Impact properties, phase structure, compatibility, and fracture morphology of polyamide-1010/thermoplastic poly(ester urethane) elastomer blends. J Polym Sci Part B Polym Phys 43:1177–1185. https://doi.org/10.1002/polb.20410

30. Chiu H-T, Chuang C-Y (2009) The mechanical and rheological behavior of the PA/TPU Blend with POE-g-MA Modifier. J Appl Polym Sci 115:1278–1282. https://doi.org/10.1002/app.30944

31. Rashmi BJ, Loux C, Prashantha K (2017) Bio-based thermoplastic polyurethane and polyamide 11 bioalloys with excellent shape memory behavior. J Appl Polym Sci 134:1–10. https://doi.org/10.1002/app.44794

32. Zhou S, Huang J, Zhang Q (2012) Mechanical and tribological properties of polyamide-based composites modified by thermoplastic polyurethane. J Thermoplast Compos Mater 27:18–34. https://doi.org/10.1177/0892705712439565

33. John B, Furukawa M (2012) Structure and mechanical behaviors of thermoplastic polyurethane thin film coated polyamide 6 fibers part II. A solution coating method. J Polym Res 19:1–12. https://doi.org/10.1007/s10965-011-9764-6

34. Genovese A, Shanks R. (2001) Simulation of the specific interactions between polyamide-6 and a thermoplastic polyurethane. Comput Theor Polym Sci 11:57–62. https://doi.org/10.1016/S1089-3156(99)00059-8

35. Zo HJ, Joo SH, Kim T, et al (2014) Enhanced mechanical and thermal properties of carbon fiber composites with polyamide and thermoplastic polyurethane blends. Fibers Polym 15:1071–1077. https://doi.org/10.1007/s12221-014-1071-5

36. Sichina WJ (2000) DSC as problem solving tool: measurement of percent crystallinity of thermoplastics

37. Schick C (2009) Differential scanning calorimetry (DSC) of semicrystalline polymers. Anal Bioanal Chem 395:1589–1611. https://doi.org/10.1007/s00216-009-3169-y

38. Millot C, Fillot L., Lame O, et al (2015) Assessment of polyamide-6 crystallinity by DSC: Temperature dependence of the melting enthalpy. J Therm Anal Calorim 122:307–314. https://doi.org/10.1007/s10973-015-4670-5

39. Stankowski M, Kropidłowska A, Gazda M, Haponiuk JT (2008) Properties of polyamide 6 and thermoplastic polyurethane blends containing modified montmorillonites. J Therm Anal Calorim 94:817–823. https://doi.org/10.1007/s10973-007-8886-x

40. Frick A, Rochman A (2004) Characterization of TPU-elastomers by thermal analysis (DSC). Polym Test 23:413–417. https://doi.org/10.1016/j.polymertesting.2003.09.013

41. John B, Furukawa M (2009) Enhanced Mechanical Properties of Polyamide 6 Fibers Coated with a Polyurethane Thin Film. Polym Eng Sci 47:1970–1978. https://doi.org/10.1002/pen.21432

42. S. Murase, M. Kashima, K. Kudo, M. Hirami (1997) Structure and properties of high-speed spun

fibers of nylon 6. Macromol Chem Phys 198:561–572. https://doi.org/10.1002/macp.1997.021980228

43. Liu L, Wu Y, Zhu Z (2017) Internal structure and crystallinity investigation of segmented thermoplastic polyurethane elastomer degradation in supercritical methanol. Polym Degrad Stab 140:17–24. https://doi.org/10.1016/j.polymdegradstab.2017.03.003

44. Hepperle J (2008) Rheological Properties of Polymer Melts. In: Kohlgrüber K (ed) Co-Rotating Twin-Screw Extruders: Fundamentals, Technology and Applications. Hanser Publishers, Munich, pp 35–45

45. Tavanaie MA, Shoushtari AM, Goharpey F, Mojtahedi MR (2013) Matrix-fibril morphology development of polypropylene / poly (butylenes terephthalate) blend fibers at different zones of melt spinning process and its relation to mechanical properties. Fibers Polym 14:396–404. https://doi.org/10.1007/s12221-013-0396-9

46. He H, Chen L, Sun S, et al (2014) Study on the matrix-fibril morphologies of polypropylene/polystyrene blends under non-isothermal uniaxial elongational flow. Fibers Polym 15:744–752. https://doi.org/10.1007/s12221-014-0744-4

47. Tang H, Wrobel LC, Fan Z (2003) Fluid flow aspects of twin-screw extruder process: numerical simulations of TSE rheomixing. Model Simul Mater Sci Eng 11:771–790. https://doi.org/10.1088/0965-0393/11/5/305

48. Martin C (2013) Twin Screw Extrusion for Pharmaceutical Processes. In: Repka M., Langley N, DiNunzio J (eds) Melt Extrusion; Materials, Technology and Drug Product Design. Springer, pp 47–79

49. Kirchhoff J (2007) Mixing and Dispersing : Principles. In: Kohlgrüber K (ed) Co-Rotating Twin-Screw Extruders: Fundamentals, Technology and Applications. Carl Hanser Publisher, pp 159–179

50. Lu G, Kalyon DM, Yilgör I, Yilgör E (2003) Rheology and extrusion of medical-grade thermoplastic polyurethane. Polym Eng Sci 43:1863–1877. https://doi.org/10.1002/pen.10158

51. Todros S, Venturato C, Natali AN, et al (2014) Effect of steam on structure and mechanical properties of biomedical block copolymers. J Polym Sci Part B Polym Phys 52:1337–1346. https://doi.org/10.1002/polb.23567

52. John B, Kojio K, Furukawa M (2009) High Performance Polyamide 6 Fibers Using Polycarbonate Based Thermoplastic Polyurethane Thin Film Coatings- a Novel Method. Polym J 41:319–326. https://doi.org/10.1295/polymj.pj2008286

53. Eltahir YA, A.M. Saeed H, Xia Y, et al (2016) Mechanical properties, moisture absorption, and dyeability of polyamide 5,6 fibers. J Text Inst 107:208–214. https://doi.org/10.1080/00405000.2015.1020678